Engineering waveguide-cavity resonant side coupling in a dynamically tunable ultracompact photonic crystal filter

Lan-Lan Lin and Zhi-Yuan Li*
Institute of Physics, Chinese Academy of Sciences, P. O. Box 603, Beijing 100080, China

Bin Lin
Department of Physics, University of Notre Dame, Notre Dame, Indiana 46556, USA
(Received 28 March 2005; revised manuscript received 20 July 2005; published 20 October 2005)

We employ a plane-wave-based transfer-matrix method in combination with a Bloch-mode scattering model to scrutinize the optical performance of an ultracompact photonic crystal (PC) all-pass optical filter made from a single-mode PC waveguide side coupled with latitudinal optical microcavities. A series of geometrical configurations of resonant microcavities side coupled with the PC waveguide, such as single one-side and two-side, periodically cascaded one-side and two-side arrangement of microcavities, and different quantities of the latitudinal and longitudinal cavity scales, cavity-cavity distance, and cavity-waveguide distance have been systematically investigated. The calculated reflection spectra exhibit a continually splitting feature of resonant frequency when the cavity size is increased. The resonant frequency shifts toward higher frequencies when we reduce the indirect coupling coefficient by increasing the waveguide-cavity distance or by introducing a symmetric two-side structure of microcavities. Optical monomode operation of the reflection pulse can be achieved for appropriate distance between two horizontal microcavities. The resonant peaks gradually evolve into a distinct rectangular shape when we introduce periodically cascaded side-coupled microcavities along the waveguide direction, implying the creation of a forbidden minigap within the guided mode continuum. The optical filter in the two-side configurations has a better filtering performance than in the one-side constructions. The cascaded side-coupled cavity-waveguide structure can act as a high-performance optical delay line.

DOI: 10.1103/PhysRevB.72.165330 PACS number(s): 42.70.Qs, 41.20.Jb, 78.67.−n

I. INTRODUCTION

Photonic crystals (PCs) are materials composed of spatially periodic arranges of dielectric and metallic building blocks.[1,2] The existence of the photonic band gap provides a newfangled channel to manipulate the flow of electromagnetic (EM) waves. Such splendid optoelectronic competency stimulates a far-reaching potential power as the platform for future all-optical ultrasmall, ultrafast integrated circuits. Some interesting applications include high efficiency beam splitting polarizer,[3] Kerr nonlinear optical laser switches,[4,5] tunable light-emitting diodes,[6,7] low-loss light waveguide,[8–14] zero-threshold laser,[15–17] omnidirectional mirrors,[18] high-speed channel multiplexers and demultiplexers,[19–22] and so on. Many of these elements and devices are realized by inserting the structural line (waveguides) and point defects (microcavities) into two-dimensional (2D) and three-dimensional (3D) photonic crystal structures.

Recently, there has been extensive interest both theoretically and experimentally in manufacturing ultracompact optical filters based on high quality-factor (Q-factor) PC microcavities that are resonantly coupled with PC waveguide channels.[19–29] These filters are capable of selecting a single signal channel with a narrow line width. They have been deliberately analyzed by the group theoretical approach, coupled-mode theory, and the finite-difference time-domain technique.[30,31] Different schemes towards realization of these optical filters, such as microring notch filters,[32] Fabry-Perot filters,[33] side-coupled ring resonator,[34] wavelength conversion,[35] high-order integrated dense switchable wave-division multiplexer and demultiplexer,[36,37] have been systematically discussed and explored in $Si-SiO_2$, GaAs-AlGaAs, GaInAsP-InP photonic crystal systems. A high-Q microcavity can also offer a good physical platform to study the quantum electrodynamics problem of atoms and molecules.[38–42]

A wide variety of numerical and theoretical methods have been developed in literatures to understand the intrinsic photon propagation behavior within 2D and 3D PC elements and devices. These include the conventional plane-wave expansion method,[43–45] real-space transfer-matrix method[46] and plane-wave-based transfer-matrix method (PWTMM),[47–51] finite-difference time-domain approach,[30,31] and Korringa-Kohn-Rostoker method.[52–54] In this paper, we will present a systematic quantitative analysis by means of the PWTMM on the optical properties of an ultracompact wavelength-selective optical filter which operates based on the resonant coupling of photonic state propagating in the single-mode PC waveguide with microcavities through the evanescent optical field in the lateral direction. For brevity, we only consider 2D PC structures. The PWTMM can conveniently handle the Bloch-mode scattering problem in semi-infinite PC structures, and therefore it allows one to accurately extract the intrinsic optoelectronic properties of functional elements and devices that are embedded in a large-scale PC environment.[48–51] The usage of deliberate Fourier analysis techniques guarantees fast numerical convergency.

The rest of this paper is arranged as follows. In Sec. II we will briefly describe the PWTMM in solution to the scatter-

ing problem of guided waves in a single-mode PC waveguide by a microcavity and the corresponding transmission and reflection spectra. In Sec. III we will discuss the continually splitting feature of a simple optical filter constructed by one PC waveguide side coupled to a single resonant microcavity with different sizes. We also consider coupling between the waveguide and two resonant microcavities that are symmetrical with respect to the waveguide axis. In Sec. IV we will investigate an optical filter made from a waveguide side coupled with two latitudinal optical microcavities. We will scrutinize the optical monomode reflection pulse balance condition through modifying the separation between the two microcavities. In Sec. V we will further examine optical filters made from cascaded multiple microcavities that are side coupled with the central waveguide. Both one-side and two-side situations will be discussed. Finally we will summarize the results of this paper in Sec. VI.

II. PWTMM SOLUTION TO SCATTERING SPECTRA IN PC OPTICAL FILTERS

The optical filter we consider is built from a microcavity side coupled with a waveguide, both of which are embedded in a 2D photonic crystal with a complete band gap. When an incident guided wave passes through the cavity region, complex scattering phenomenon happens and the central problem is to find out the reflection and transmission coefficients of the guided wave. The PWTMM has a great advantage in solution to this problem because it can handle conveniently the guided wave scattering in semi-infinite PC structures and thus avoid the complex multiple reflection effect involved in a finite-length sample.

The physical model to simulate the ultracompact wavelength-selective filters can be schematically depicted in Fig. 1(a). It consists of two semi-infinite PC waveguide (denoted as PC1 and PC2) connected by the central sandwiched scattering domain involving microcavities. For the current guided-wave scattering problem where the EM field is well localized around the waveguide and cavity, we can use a supercell technique to simulate the real problem. The approximation is quite satisfactory provided that the separation between the adjacent waveguides in the lateral direction is sufficiently large. In the PWTMM, we first solve the eigenmode of the transfer matrix of the two semi-infinite PC waveguides by expanding the EM fields into plane waves associated with the supercell. The resulting eigenmodes are described by column vectors $\Pi^{\pm}$ and $\Sigma^{\pm}$, respectively. In the eigenmode space we can conveniently and elegantly discuss the modulation of these eigenmodes by any scattering objects. Assume that the eigenvector matrix in the plane-wave space for PC1 and PC2 is S_1 and S_2, and the scattering matrix connecting the fields at the surface of PC1 and PC2 is S_a, then the transmission eigenmode vector Σ_0^+ and the reflection eigenmode vector Π_0^- under the excitation of an incident eigenmode vector Π_0^+ can be solved by the following linear equation:

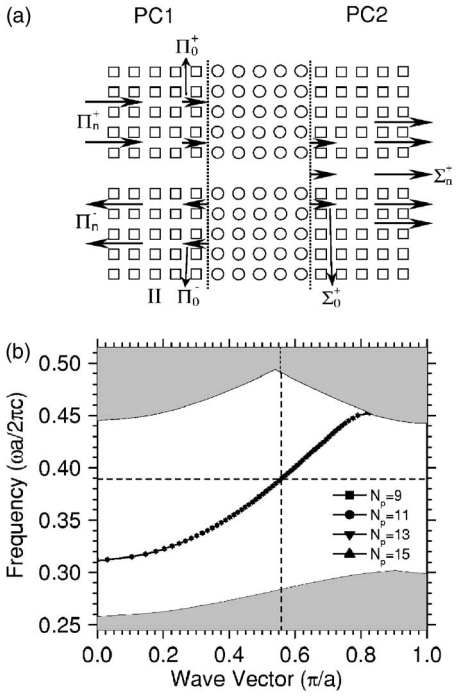

FIG. 1. (a) The schematic geometric configuration to solve the scattering problem of incident guided wave in an all-optical wavelength-selective filter embedded in 2D square lattice photonic crystal. The input and output arms of waveguide channel (PC1 and PC2) are assumed to be semi-infinite. The sandwiched domain represents the microcavity region. $\Pi_0^{\pm}$ and Σ_0^+ are eigenmode vectors at the surface of PC1 and PC2, while $\Pi_n^{\pm}$ and Σ_n^+ are eigenmode vectors far from the surface. (b) The calculated dispersion diagram for the single guided mode (solid line) supported by a single-missing-row waveguide created in the photonic crystal. The upper and lower gray areas correspond to the upper and lower photonic bands. Different plane wave numbers (N_p per unit cell) have been adopted. The cross point of two dashed lines is the operation frequency $\omega=0.38913(2\pi c/a)$ at which monomode emission of two coupled cavities is achieved.

$$\begin{pmatrix} S_2^{(11)} - S_a^{(12)}S_2^{(21)} & -S_a^{(11)}S_1^{(12)} \\ -S_a^{(22)}S_2^{(21)} & S_1^{(22)} - S_a^{(21)}S_1^{(12)} \end{pmatrix} \begin{pmatrix} \Sigma_0^+ \\ \Pi_0^- \end{pmatrix} = \begin{pmatrix} S_a^{(11)}S_1^{(11)}\Pi_0^+ \\ [S_a^{(21)}S_1^{(11)} - S_1^{(21)}]\Pi_0^+ \end{pmatrix}. \quad (1)$$

In Eq. (1), $S_1^{(ij)}$, $S_2^{(ij)}$, and $S_a^{(ij)}$ $(i,j=1,2)$ are the block submatrices of the matrix S_1, S_2, and S_a, respectively. The unknown variables Σ_0^+ and Π_0^- represent the transmission and reflection fields (in the eigenmode space). From these column vectors, we can find the coefficients of the incident, reflection, and transmission guided waves of the single-mode PC waveguide PC1 and PC2. Then we return back to the plane-wave space and calculate the plane-wave coefficient column vectors, from which the reflection and transmission coefficients of the guided wave can be straightforward obtained. At this step the solution to the scattering problem by means of the Bloch-mode scattering method has been com-

pleted. For more mathematical and technical details about this model, see Ref. 49.

III. CONTINUALLY FREQUENCY SPLITTING WITH INCREASING MICROCAVITY SIZE

The optical filter we study is built in the 2D PC made from a square lattice of dielectric cylinders in air. The cylinder has a dielectric constant of $\epsilon=11.56$ and radius $r=0.18a$, where a is the lattice constant. A single-mode waveguide is created by removing one single row of dielectric rods along the (10) crystalline direction. The calculated dispersion diagram of the guided mode propagating in the PC waveguide is illustrated in Fig. 1(b). The background bulk PC exhibits a TM-polarization (where the electric field is parallel to the axis of the cylinder) band gap at $0.258 \leqslant \omega \leqslant 0.444$ [in unit of $(2\pi c/a)$, where c is the light speed in vacuum]. The waveguide supports a single wide band of guided mode spanning from 0.312 to the upper band edge. In the simulations, a supercell involving 9 unit cells is used to model the PC waveguide, and different plane numbers (9, 11, 13, and 15 plane waves per unit cell) are adopted to see the convergency behavior of the PWTMM. The numerical convergency is very excellent, and we see almost no difference in the four dispersion curves. For instance, at $\omega=0.35$, the corresponding wave vector k is 0.38899, 0.38909, 0.38912, and 0.38914 (π/a) for 9, 11, 13, and 15 plane waves per unit cell, respectively. At $\omega=0.4$, k is 0.59719, 0.59725, 0.59728, and 0.59729 (π/a) for 9, 11, 13, and 15 plane waves per unit cell, respectively. It is seen that the usage of 11 plane waves per unit cell has already led to a good enough numerical convergency (better than 0.5%) for the considered TM polarization mode. Therefore, we have adopted 11 plane waves per unit cell in our simulations all throughout this paper. This high numerical accuracy is consistent with the well-known fact that the EM field is continuous everywhere in the whole structure, and this guarantees fast convergence and high accuracy of numerical simulation.

The optical microcavity can be generated by removing one or several (number N_{MC}) dielectric cylinders in the neighborhood of the waveguide along the (10) direction (parallel to the waveguide). The microcavity has a size of $N_{MC}a$, and the longitudinal center-to-center distance between the waveguide and microcavity is s. We call this type of filter a one-side filter. One might also introduce more identical microcavities alternatively along the (10) direction with equal center-to-center separation as d, and it is called a cascaded-cavity filter. Besides, another symmetric set of microcavities can also be created in the opposite side of the waveguide axis, leading to a new type of filter called a two-side filter.

As schematically illustrated in Fig. 1(a), when an incident guided wave impinges from left to right along the waveguide and encounters the microcavity domain, it is tapped by the resonant microcavity aided by the evanescent optical field penetrating through the waveguide wall. After excitation, the cavity mode can reradiate EM fields back to the waveguide continuum, and form the forward transmission and backward reflection wave signals. We first consider the scattering of the incident guided wave by an isolated resonant microcavity with a longitudinal distance s from the common bus of a, $2a$, and $3a$, respectively.

The ultracompact optical filter can completely transfer the energy through the direct resonant coupling between different microcavity modes and indirect coupling between the propagating continuum and localized microcavity modes. To see the physics clearly, we consider a simple optical filter involving only one microcavity mode coupled with the waveguide continuum states. In this element, one only needs to account for the indirect interaction assisted by the evanescent optical field. Following the theoretical analysis presented in Ref. 22, the amplitude of the reflection and transmission coefficients r and t and the total decay rate of the mode $|n\rangle$ can be explicitly written as

$$r = -i\sum_n \frac{1}{\omega_k - \omega_n + i\Gamma_n}\frac{LV_{-k,n}V_{n,k}}{v_g}, \tag{2}$$

$$t = 1 - i\sum_n \frac{1}{\omega_k - \omega_n + i\Gamma_n}\frac{L|V_{-k,n}|^2}{v_g}, \tag{3}$$

$$\Gamma_n = \Gamma_n^0 + \frac{L(|V_{k,n}|^2 + |V_{-k,n}|^2)}{2v_g} = \Gamma_n^0 + \Gamma_n^c, \tag{4}$$

where ω_k and ω_n are the resonant frequencies of the continuum guided state and localized microcavity modes, V_g is the group velocity amplitude, Γ_n^0 represents the intrinsic loss (gain) of the optical resonator, Γ_n^c represents the decay loss into the guided-wave mode, Γ_n is the total mode decay rate, and L is the waveguide length. The coefficients $V_{k,n}$ and $V_{-k,n}$ monitor the coupling strength between a localized state $|n\rangle$ and the forward and backward propagating states $|k\rangle$ and $|-k\rangle$, respectively. In the current situation, the microcavity possesses the mirror symmetry with respect to the $x=0$ plane passing through the center of the cavity, $V_{k,n}=V_{-k,n}^*$, so we can find $\Gamma_n^c = L|V_{k,n}|^2/v_g$. The power reflection coefficient R and transmission coefficient T can be further simplified:

$$R = |r|^2 = \frac{(\Gamma_n^c)^2}{\Delta\omega^2 + (\Gamma_n^0 + \Gamma_n^c)^2}, \tag{5}$$

$$T = |t|^2 = \frac{\Delta\omega^2 + (\Gamma^0)^2}{\Delta\omega^2 + (\Gamma_n^0 + \Gamma_n^c)^2}. \tag{6}$$

Here $\Delta\omega$ is $\omega-\Omega$, with ω being the frequency of the incident light and Ω the cavity-mode resonant frequency. In addition, we assume no intrinsic loss or gain in the system, so $\Gamma_0=0$. Then Eqs. (5) and (6) become

$$R = |r|^2 = \frac{(\Gamma_n^c)^2}{\Delta\omega^2 + (\Gamma_n^c)^2}, \tag{7}$$

$$T = |t|^2 = \frac{\Delta\omega^2}{\Delta\omega^2 + (\Gamma_n^c)^2}. \tag{8}$$

Obviously the reflection spectrum follows a Lorentzian line shape of resonance peak. At the resonance, $\Delta\omega=0$, we have

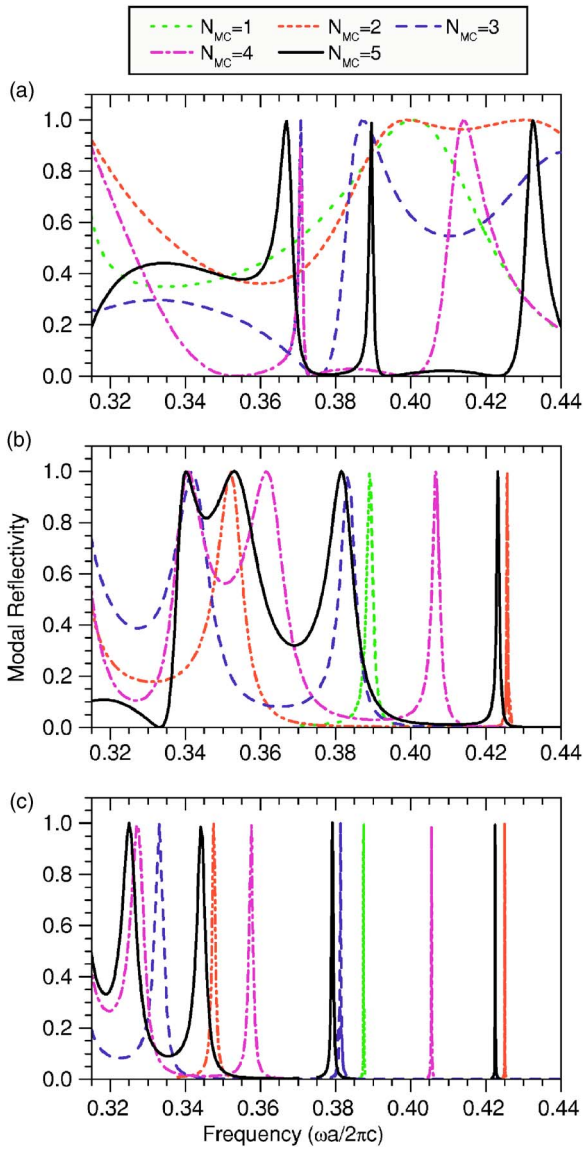

FIG. 2. (Color online) Calculated reflection spectra of an ultracompact PC filter consisting of a single microcavity side-coupled with the central channel waveguide. The longitudinal waveguide-cavity distance is (a) $s=a$, (b) $s=2a$, and (c) $s=3a$, respectively. In each panel, different numbers of missing rods in the cavity along the latitudinal direction as $N_{MC}=1$ to 5 are considered.

unity reflection coefficient $R=1$ and zero transmission coefficient $T=0$.

The calculated TM-mode reflection spectra around the resonance frequency are displayed in Figs. 2(a)–2(c) for a single microcavity formed by continually removing 1, 2, 3, 4, and 5 dielectric cylinders along the (10) direction at a longitudinal distance s of a, $2a$, and $3a$, respectively. The resonant reflection spectra for all the geometric configurations exhibit a Lorentzian line shape. The backward reflection signal supported by the microcavity with a latitudinal size of a is resonant at 0.40032, 0.3890, and 0.3875 [in unit of $2\pi c/a$] at $s=a$, $2a$, and $3a$, respectively. The resonance peak exhibits a reducing line width [measured by the full width at half maximum (FWHM)] and increasing Q-factor with the growing distance s. The reason is simple: The waveguide-cavity coupling becomes weaker for larger s, leading to a continually reduction in the decay rate of the cavity mode. The Q factor can be numerically calculated from the exponential decay rate of the resonant mode inside the microcavity:

$$Q = \frac{\omega_c E}{P} = \frac{\omega_c E}{\frac{\partial E}{\partial t}} = \frac{\omega_c}{\Delta\omega}, \tag{9}$$

where E is the stored energy, $P=\partial E/\partial t$ the dissipated power, ω_c the resonant frequency, and $\Delta\omega$ the FWHM of the reflection peak.

The resonant frequency of the reflected wave exhibits a continually splitting feature with the increasing number of missing dielectric cylinders. The filter of $s=a$ reflects the incident signal resonant at the frequency of 0.40032 for the single missing rod microcavity ($N_{MC}=1$). With the increase of cavity size, continual split of the resonant frequency is observed. The reflection pulse from the $N_{MC}=2$ filter shows two resonant peaks located at frequencies 0.399 and 0.430, respectively. The reflection signal of the optical filter with $N_{MC}=3$, 4, 5 exhibits one, two, and three resonant peaks, and they are located at 0.387 ($N_{MC}=3$), 0.3707 and 0.414 ($N_{MC}=4$), and 0.367, 0.3895, and 0.4325 ($N_{MC}=5$), respectively. Generally speaking, high-efficiency all-optical filters intrinsically demand a high resonant Q-factor to implement high filtering resolution. The Q-factor of the reflection peak located at the highest frequency increases from 7.27 to 77.23 as the microcavity size grows from a to $5a$. The maximum values of the Q-factor can reach 314 and 309 for the two narrow resonant peaks located at 0.3707 and 0.3895 in the $N_{MC}=4$ and 5 filters, respectively.

It is distinct from Fig. 2(b) that when the vertical waveguide-cavity distance s is increased, the reflection spectra show a more explicit splitting characteristic. This feature can be ascribed to the exponentially decay of the indirect coupling coefficients as a function of the distance s. Furthermore, the resonant frequency gradually shifts towards the low frequency direction and the line width of the resonant peak becomes increasingly narrower. In all situations, the reflection resonant signals exhibit a Lorentzian line shape that is well described by Eq. (7). The Q-factor of the reflection pulse emitted from the localized microcavity at $s=3a$ as illustrated in Fig. 2(c) increases by approximately 5–15 times compared with those optical filters with $s=a$. The maximum Q-factor can reach 8674 for the resonant peak located at 0.425 in the $N_{MC}=2$ filter. Generally speaking, the longer the longitudinal waveguide-cavity distance s, the higher the Q-factor is. Nevertheless, increasing the distance s may weaken the energy transfer efficiency of the output signal from the optical filter. Therefore, it is important to find an optimum structure to achieve a balance between the Q-factor and the output efficiency. In this regard, the $s=2$ filters might fit for this purpose. Such an all-pass optical filter can be greatly advantageous to transfer the ultrashort optical pulse to build the high-speed all-optical time-domain demultiplexing system with a bit rate of 1T bit/s, which requires an optical delay time of approximately 1 ps.

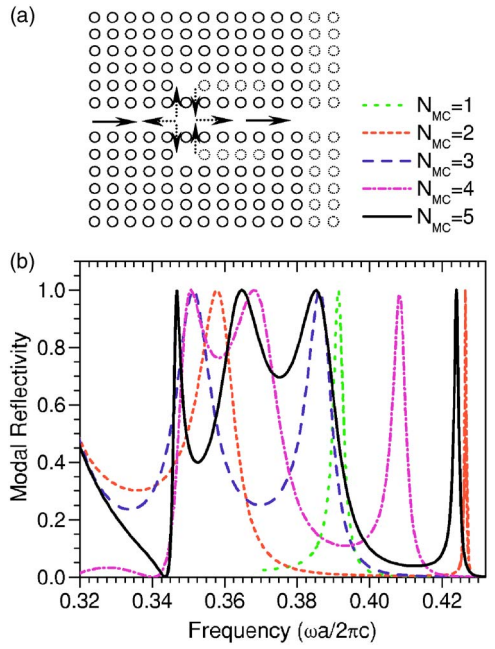

FIG. 3. (Color online) (a) The schematic representation of the geometric architecture and (b) the resonant reflection spectra of an optical filter involving a pair of two-side symmetric microcavities side-coupled with the single mode PC waveguide. Different numbers of missing rods in the cavity along the latitudinal direction as $N_{MC}=1$ to 5 are considered.

Although the optimal FWHM value of the optical reflection signal from the isolated side-coupled microcavity can be achieved to diminish the power dissipation, one still needs to take into account another important feature of an ideal filter: The intensity of reflected pulse should amount to 99.999% to guarantee the complete energy transfer and excellent output signal efficiency. For this purpose, we have conducted more deliberate investigations on the impacts of the enhanced indirect resonant coupling characteristic between the localized microcavity state and the channel continuum mode via inserting a second microcavity which is identical to the original one but is placed symmetrically in the opposite side of the channel waveguide. The two-side symmetric microcavities might underscore the indirect resonant coupling coefficient in the filter. The schematic geometry of the double indirect side-coupled microcavity-waveguide system is illustrated in Fig. 3(a). The two resonant microcavities possess two-fold symmetries with respect to the mirror planes parallel and perpendicular to the channel waveguide.

The calculated reflection spectra of the two side-coupled optical filters with parameters N_{MC} from 1 to 5 and $s=2a$ are displayed in Fig. 3(b). In comparison with the reflection spectra for the filters of single side-coupled optical microcavity as shown in Fig. 2(b), the resonance reflection of the current filter happens at the higher frequency regime and the energy transfer efficiency enhances significantly. The average increment of the resonant frequency is 0.0043 and the Q-factor declines approximately to one half compared with the single side-coupled filter. The continual blue shift of the central resonant frequency implies that the even state among the two coupled cavity modes participates in the excitation of the optical filter by the incident even-mode guided wave. Noteworthy is that the energy transfer efficiencies of all reflection pulses surmount to 99.9999% in the optical filters. This suggests that the intensively enhanced indirect resonant coupling between the channel waveguide mode and localized microcavity modes would make a considerable contribution to elevate the energy transfer efficiency.

IV. REFLECTION SPECTRA AND BALANCE CONDITIONS OF COMPLETE SIGNAL TRANSFER IN SIDE-COUPLED FILTERS

We proceed to consider a more complex optical filter that involves multiple resonators simultaneously in direct and indirect coupling with the waveguide continuum. The filter is simply made by introducing second microcavity in the neighborhood of the first microcavity along the (10) direction and parallel to the waveguide axis, as shown in Fig. 4(a). Following Ref. 21, the resonant frequency and decay rate of the resonant state for this new filter can be derived explicitly as follows:

$$\tilde{\omega}_{\text{even}} = \omega_0 + V_x - \frac{|V_{q_0}|^2}{g_0}\sin(q_0 d), \tag{10}$$

$$\tilde{\omega}_{\text{odd}} = \omega_0 - V_x + \frac{|V_{q_0}|^2}{g_0}\sin(q_0 d), \tag{11}$$

$$\gamma_{\text{even}} = \frac{|\cos(q_0 d/2)V_{q_0}|^2}{g_0}, \tag{12}$$

$$\gamma_{\text{odd}} = \frac{|\sin(q_0 d/2)V_{q_0}|^2}{g_0}. \tag{13}$$

Here q_0 and g_0 are the wave vector and group velocity of the guided wave at the resonant frequency, V_x is the coupling strength between two localized cavity states $|c_1\rangle$ and $|c_2\rangle$, V_{q_0} the coupling between the propagating state $|q_0\rangle$ and localized $|c\rangle$ state, and d is the interval between the two microcavities. The first and second terms on the right side of Eq. (10) represent the direct and indirect coupling mechanism, respectively. In order to realize the complete energy flux transfer from the incident propagating state to the backward propagating state, the resonant frequency and line width of the states should be equal in magnitude.[21] This condition requests that the following kinetic relations be satisfied:

$$q_0 d = (n + 1/2)\pi, \tag{14}$$

$$V_x - \frac{|V_{q_0}|^2}{g_0}\sin(q_0 d) = 0. \tag{15}$$

In Eq. (14) n is an integer. The resonant frequency does not split when Eq. (15) is satisfied. Equation (14) can be further expressed as the following laws when the decay rate of the even and odd resonant supermodes for the coupled cavities happens to be equal:[21]

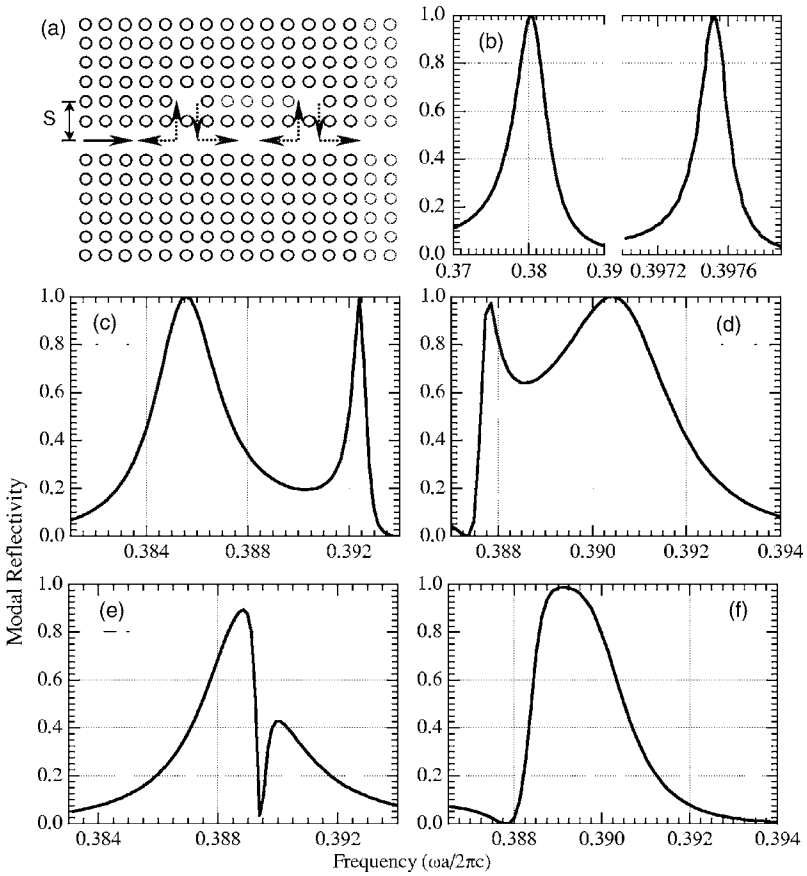

FIG. 4. (a) The schematic geometric configuration of an optical filter involving two latitudinally coupled optical one-missing-rod microcavities side-coupled with the single mode PC waveguide. The curves in (b)–(f) are the calculated resonant reflection spectra of the filter where the two cavities are separated by a, $2a$, $3a$, $4a$, and $5a$, respectively. The longitudinal cavity-waveguide distance is $s=2a$.

$$q_0 d = 2\pi(n + 1/4) \quad \text{for even symmetry}, \tag{16a}$$

$$q_0 d = 2\pi(n + 3/4) \quad \text{for odd symmetry}. \tag{16b}$$

Here the symmetry is with respect to the mirror plane bisecting the line connecting the center of the two cavities.

The calculated reflection spectra of the all-optical filter consisting of two horizontal side-coupled microcavities with the separation distance d from a to $5a$ and a longitudinal distance of $s=a$ are illustrated in Figs. 4(b)–4(f). The two coupled microcavities support two resonant cavity modes which are located at frequency 0.3803 and 0.3975, respectively. The Q-factor of the reflection signal resonating at frequency 0.3975 is dramatically enhanced to a high value of 2028, ten times larger than the value in the monopole resonator as shown in Fig. 2(b). The splitting of the resonant frequency and the enhancement of the Q-factor can be attributed to the introduction of a direct coupling interaction V_x between two localized cavity states $|1\rangle$ and $|2\rangle$. With the increasing d, the direct coupling coefficient V_x decreases exponentially due to the decaying nature of the localized wave functions.

The FWHM of the resonant reflection signals increases significantly and there appears hyperfine splitting of resonant frequency in the quasi-flat impurity band as shown in Fig. 4(c). Figure 4(f) clearly shows that the splitting disappears when d is equal to $5a$, leading to the single mode operation that is highly expected for a high efficiency and low power loss filter. At the monomode emission, the resonant frequency is 0.38913, and the Q-factor is 185.2, and they are very close to the values 0.389 and 208 for the isolated microcavity resonator as shown in Fig. 2(c). The reflection spectrum around resonance for the two-cavity filter at $d=5a$ can be approximately described by a super-Lorentzian line shape, and this indicates excellent signal transfer and output with a minimized power loss. The resonant frequency of this optical filter is found to be 0.38913, and the corresponding guided mode has a wave vector q_0 as $0.554(\pi/a)$, according to the dispersion diagram as illustrated in Fig. 1(b) by the cross dashed lines. Substituting the calculated values of the resonant frequency and wave vector into Eq. (16b), we can find that the value of n is approximately equal to 1, and this corresponds to the odd-symmetric supermode for the coupled cavities.

In order to acquire a more clarified insight into the resonant dynamics and the optical properties of the ultrasmall PC optical filter, we construct latitudinal cascaded side-coupled resonant microcavities with an equal horizontal separation of $5a$ along the (10) direction between adjacent cavities and a vertical distance $s=2a$ from the waveguide channel. The geometric configuration of the designed side-coupled cascaded-cavity all-pass filters is schematically illuminated in Fig. 5(a).

The direct coupling between the cascaded microcavities should also result from the evanescent optical field. The calculated reflection spectra for an incident guided wave upon the cascaded-cavity filter containing 1, 2, 3, 4, and 8 side-coupled resonant microcavities are illustrated in Fig. 5(b). When more cavities are involved in the filter, the resonant

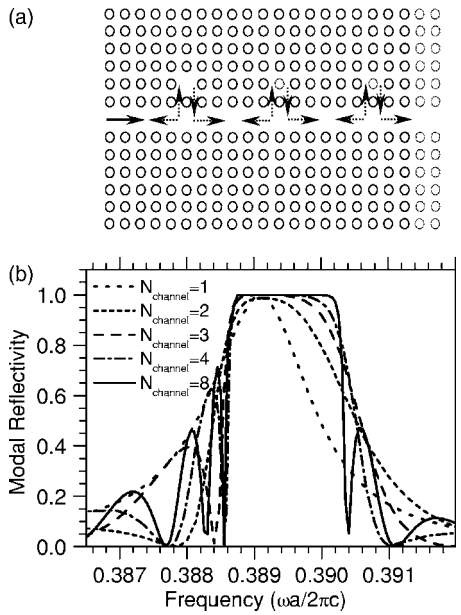

FIG. 5. (a) The schematic geometric configuration of an optical filter involving a series of periodically cascaded one-missing-rod microcavities side-coupled with the single mode PC waveguide. The distance between adjacent cavities is $5a$, and the longitudinal cavity-waveguide distance is $s=2a$. (b) Calculated resonant reflection spectra of the filter where $N_{\text{channel}}=1$, 2, 3, 4, and 8 cavities are involved in the one-side cascaded-cavity filter.

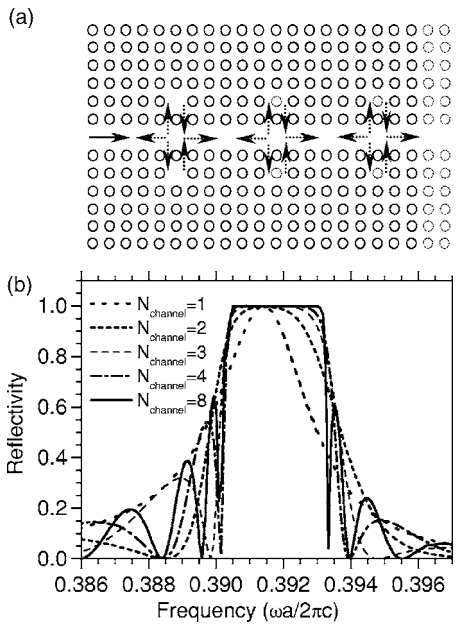

FIG. 6. (a) The schematic geometric configuration of an optical filter involving a series of periodically cascaded one-missing-rod microcavities coupled with the single mode PC waveguide symmetrically in the two sides. The distance between adjacent cavities is $5a$, and the longitudinal cavity-waveguide distance is $s=2a$. (b) Calculated resonant reflection spectra of the filter where $N_{\text{channel}}=1$, 2, 3, 4, and 8 pairs of cavities are involved in the two-side cascaded-cavity filter.

reflection peak gradually widens and evolves into a wide flat plateau of reflection coefficient $R=100\%$, indicating better performance in energy transfer and output efficiency. The feature can be well explained by the multiple reflection and interference effect of the guided wave among the periodically cascaded microcavities. These effects can result in the formation of photonic bands and band gaps within the original wide guided-wave pass band. The physics is the same as those that are well-known in photonic crystals. The band gap should correspond to the flat-plateau region, and it has been in excellent shape for a filter containing 8 cascaded coupled cavities. The speedy oscillation in the reflection spectrum curve around the reflection peaks also originates from the optical interference among the multiple side-coupled resonators.

Similar to the single cavity situation as discussed in Figs. 2 and 3, we add a symmetric set of cascaded side-coupled microcavities in the opposite side of the central waveguide channel of the one-side optical filter shown in Fig. 5(a). The geometric architecture of the new cascaded-cavity filter is depicted in Fig. 6(a). The calculated reflection spectra of this filter are displayed in Fig. 6(b), where 1, 2, 3, 4, and 8 pairs of symmetric cavities are considered. The optical filter possesses a mirror symmetry with respect to the waveguide axis. It is particularly impressive that the output reflection signals of the two-side filter containing only one and two pairs of cascaded resonant microcavities have already reached 100% in a rather wide frequency window. The filtering performance is much better than the corresponding one-side filters, where the maximum reflection coefficients are only about 99%.

The resonant frequency ω_c and Q-factor of the reflection signals in the one-side and two-side cascaded optical filters as a function of the cascaded cavity number are summarized in Figs. 7(a) and 7(b), respectively. The output resonant reflection signal in the one-side filter containing 1, 2, 3, 4, and 8 microcavities is centered at frequencies 0.389, 0.38913, 0.38915, 0.38921, and 0.38945, respectively. The central resonance signal slightly moves to higher frequency when the cascaded cavity number increases. The corresponding Q-factor are found to be 208, 185, 191, 205, and 224, respectively. The resonant frequency ω_c of the two-side cascaded-cavity filter is slightly higher than the corresponding one-side cascaded-cavity filter, similar to the single-cavity situation as shown in Figs. 2 and 3. The reason is the same. The evenly symmetric incident guided wave can only couple with the even mode supported by the cascaded-cavity coupled system, which is split to the higher frequency. The two-side cascaded-cavity filter has a slightly lower Q-factor.

Finally we expand the longitudinal scale of the cascaded optical resonant microcavities from a to $2a$ by removing two dielectric rods, and see what happens to their optical performances. The geometric configuration of the optical filter is schematically demonstrated in Fig. 8(a). Now each single cavity will support two resonant cavity modes, and very complex multiple scattering effect will take place when many of these cavities are brought together. The calculated reflection spectra around the low and high resonance peaks are displayed in Figs. 8(b) and 8(c), respectively. Compared with the monomode features of the reflection spectra as illustrated in Fig. 5, the reflection signals of the cascaded-

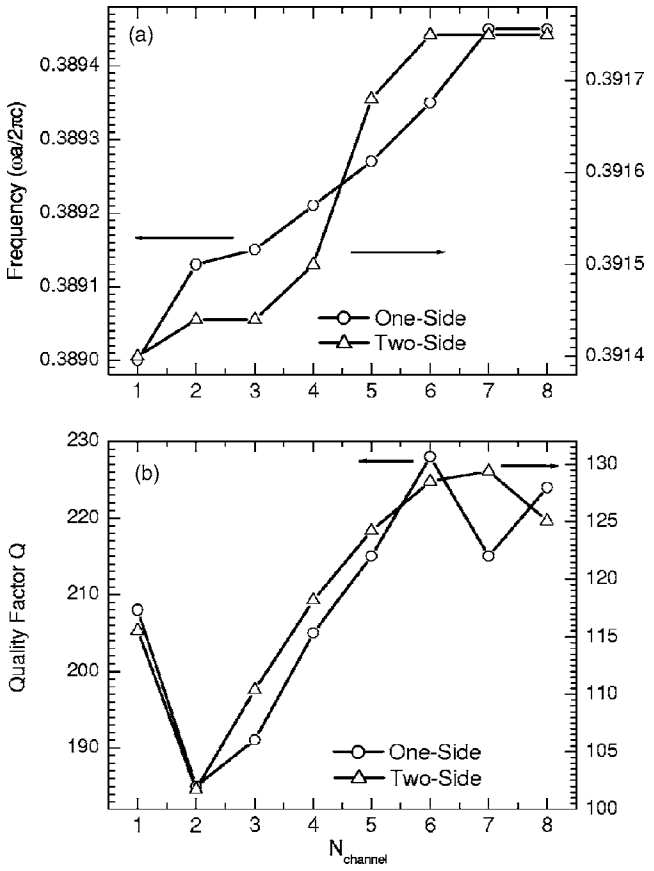

FIG. 7. The central resonant frequency (a) and corresponding Q-factor (b) of the resonant reflection peaks in the one-side and two-side cascaded-cavity optical filters as a function of the number of cavities N_{channel} that comprise the filter.

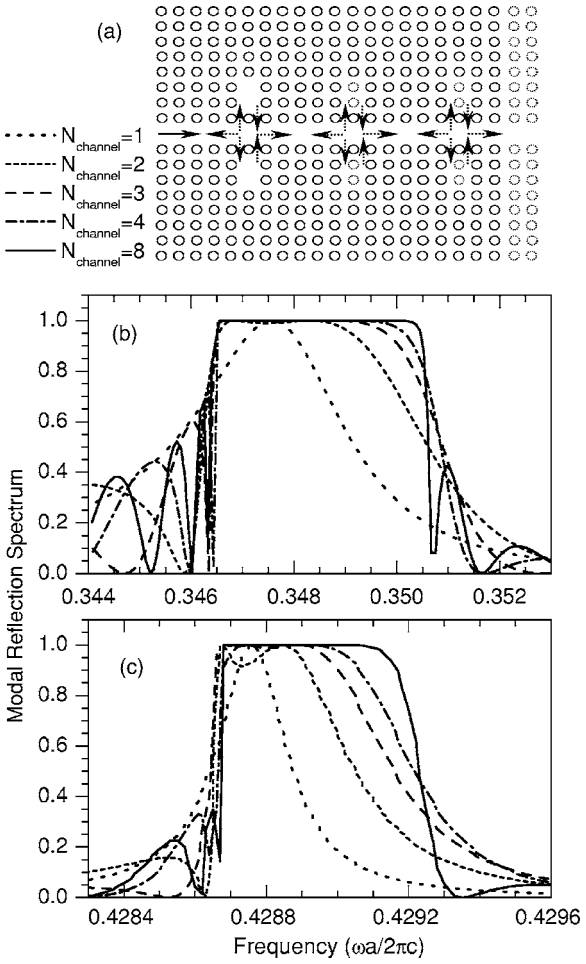

FIG. 8. (a) The schematic geometric configuration of an optical filter involving a series of periodically cascaded microcavities coupled with the single mode PC waveguide symmetrically in the two sides. The distance between adjacent cavities is $5a$, and the longitudinal cavity-waveguide distance is $s=2a$. Each cavity involves two missing rods along the longitudinal direction. Calculated resonant reflection spectra of the filter for the lower (b) and higher (c) resonant peaks. Different two-side cascaded-cavity filters made from $N_{\text{channel}}=1$, 2, 3, 4, and 8 pairs of cavities are considered.

cavity optical filter are resonant at two frequencies of about 0.348 and 0.42885, respectively. Similar to the situation of one missing-rod cavity as shown in Figs. 5 and 6, the line shape of both output reflection signals gradually approaches a sharp flat plateau with magnitude of 100%, indicating the formation of a mini band gap within the original guided-wave pass band. In addition, in the new cavity configuration, the rapid oscillation of the reflection coefficients around the reflection peaks that are originated from the optical interference of the cascaded multiple coupled cavities are suppressed to some extent. The resonant frequency and Q-factor of the reflection pulses for this optical filter as a function of the number of latitudinally cascaded microcavity pairs are shown in Figs. 9(a) and 9(b), respectively. The Q-factor of the reflection peak around frequency 0.42885 witnesses an enhancement to more than 800.

The periodically cascaded-cavity filter can serve as an optical delay line, because the coupled waveguide-cavity system can modify the wave propagation behavior such that it is significantly different from the original free PC waveguide. We have seen that Bragg scattering among the compound system consisting of the side-coupled cavities and the waveguide can create a miniband and even a band gap in the original wide band of guided wave supported by the PC waveguide. The dispersion diagram of the coupled waveguide-cavity system and the corresponding group velocity of light wave transporting through the system can be conveniently engineered by changing a wide variety of geometric and physical parameters of the system, such as the cavity-cavity distance, the cavity-waveguide distance, the latitudinal and longitudinal cavity scales, as well as the one-side or two-side nature of the cavities. The effect of many of these factors on the optical properties, in particular the filtering performance, has been discussed systematically in the above sections. The existence of miniband within the wide guided-wave band can lead to a greatly reduced group velocity and large group delay of light pulse.

V. CONCLUSION

In summary, we have employed the PWTMM, in particular the Bloch-mode scattering model to systematically investigate the optical properties of an ultracompact PC all-pass

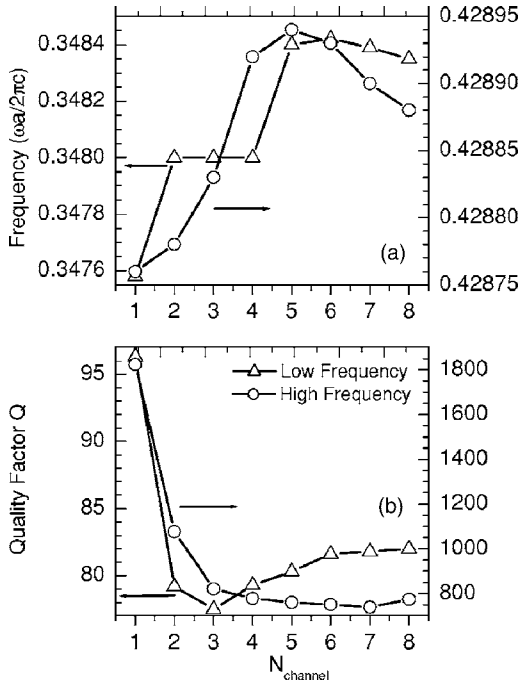

FIG. 9. The central resonant frequency (a) and corresponding Q-factor (b) of the resonant reflection peaks in the two-side two-missing-rod cascaded-cavity optical filters shown in Fig. 8 as a function of the number of cavities N_{channel} that comprise the filter.

optical filter that are built from resonant microcavities side coupled with a single mode waveguide in the platform of 2D PC structure with a complete band gap. We have considered a series of geometrical configurations of resonant microcavities side coupled with the single-mode PC waveguide. The calculated reflection spectra exhibit a continually splitting feature of resonant frequency when the cavity size is increased. This feature is associated with the direct and indirect resonant coupling mechanism between localized cavity modes, and between the propagating guided modes continuum and localized cavity modes. The resonant frequency shifts toward higher frequencies when we reduce the indirect coupling coefficient by increasing the waveguide-cavity distance or by introducing a second group of symmetric optical cavities on the opposite side of the waveguide. Optical monomode operation of the reflection pulse can be achieved for appropriate distance between two horizontal microcavities. In this case, the two coupled cavities support degenerate supermodes and the resonant peak of the original single cavity ceases to split. As a result, the reflection spectrum exhibits a super-Lorenztian line shape. The two-side symmetric microcavities filter is resonant at higher frequencies because only the even-symmetric mode can couple with the incident even-symmetric guided wave. The filter exhibits better reflection spectrum features compared with the one-side microcavities filter.

The reflection resonant peaks gradually evolve into a distinct rectangular flat plateau of magnitude 100% when we introduce more and more periodically cascaded side-coupled microcavities along the waveguide direction. This indicates the creation of a forbidden minigap within the original wide band of guided mode continuum. The reason is simply the well-known Bragg scattering effect. The filter made from two-side cascaded symmetrical microcavities resonates at higher frequency and has an improved filtering performance compared with the one-side cascaded-cavity filter, similar to the single-cavity situation. We have found that increasing the longitudinal cavity scale can significantly enhance the Q-factor and improve the optical performance of the filter. This feature should be beneficial to manipulate the ultrafast all-optical time-domain demultiplexing system. The cascaded side-coupled waveguide-cavity system can act as an efficient optical delay line because it can conveniently modify the dispersion diagram, the corresponding group velocity and group delay time of a light wave pulse via changing a wide range of geometrical and physical parameters of the microcavities.

ACKNOWLEDGMENTS

This work was supported by the National Key Basic Research Special Foundation of China under contract No. 2004CB719804 and the National Natural Science Foundation of China under the contract No. 10404036.

*Electronic address: lizy@aphy.iphy.ac.cn

[1] E. Yablonovitch, Phys. Rev. Lett. **58**, 2059 (1987).
[2] J. D. Joannopoulos, P. R. Villeneuve, and S. Fan, Nature (London) **386**, 143 (1997).
[3] D. R. Solli, C. F. McCormick, R. Y. Chiao, and J. M. Hickmann, J. Appl. Phys. **93**, 9429 (2003).
[4] M. Bahl, N. C. Panoiu, and R. M. Osgood, Jr., Phys. Rev. E **67**, 056604 (2003).
[5] A. R. McGurn and G. Birkok, Phys. Rev. B **69**, 235105 (2004).
[6] G. Veronis, W. Suh, Y. Liu, M. Han, Z. Wang, R. W. Dutton, and S. Fan, J. Appl. Phys. **97**, 044503 (2005).
[7] D. Ohnishi, T. Okano, M. Imada, and S. Noda, Opt. Express **12**, 1562 (2004).
[8] M. Notomi, K. Yamada, A. Shinya, J. Takahashi, C. Takahashi, and I. Yokohama, Phys. Rev. Lett. **87**, 253902 (2001).
[9] E. Lidorikis, M. L. Povinelli, S. G. Johnson, and J. D. Joannopoulos, Phys. Rev. Lett. **91**, 023902 (2003).
[10] H. Takeda and K. Yoshino, Phys. Rev. B **67**, 073106 (2003).
[11] M. Florescu and S. John, Phys. Rev. A **69**, 053810 (2004).
[12] O. Painter and K. Srinivasan, Phys. Rev. B **68**, 035110 (2003).
[13] S. G. Johnson, P. R. Villeneuve, S. Fan, and J. D. Joannopoulos, Phys. Rev. B **62**, 8212 (2000).
[14] P. Kramper, M. Agio, C. M. Soukoulis, A. Birner, F. Müller, R. B. Wehrspohn, U. Gösele, and V. Sandoghdar, Phys. Rev. Lett. **92**, 113903 (2004).
[15] H. G. Park, S. H. Kim, S. H. Kwon, Y. G. Ju, J. K. Yang, J. H. Baek, S. B. Kim, and Y. H. Lee, Science **305**, 1444 (2004).
[16] O. Painter, R. K. Lee, A. Scherer, A. Yariv, J. D. OBrien, P. D.

Dapkus, and I. Kim, Science **284**, 1819 (1999).
[17] J. Painter, A. Husain, A. Scherer, J. D. OBrien, I. Kim, and P. D. Dapkus, J. Lightwave Technol. **17**, 2082 (1999); S. Noda, M. Yokoyama, M. Imada, A. Chutinan, and M. Mochizuki, Science **293**, 1123 (2001).
[18] C. Hooijer, D. Lenstra, and A. Lagendijk, Opt. Express **25**, 1666 (2000).
[19] W. Jiang and R. T. Chen, Phys. Rev. Lett. **91**, 213901 (2003).
[20] S. Fan, P. R. Villeneuve, and J. D. Joannopoulos, and H. A. Haus, Phys. Rev. Lett. **80**, 960 (1998).
[21] S. Fan, P. R. Villeneuve, J. D. Joannopoulos, M. J. Khan, C. Manolatou, and H. A. Haus, Phys. Rev. B **59**, 15882 (1999).
[22] Y. Xu, Y. Li, R. K. Lee, and A. Yariv, Phys. Rev. E **62**, 7389 (2000).
[23] B. Min, J. Kim, and H. Y. Park, Appl. Phys. Lett. **86**, 011106 (2005).
[24] Y. Akahane, M. Mochizuki, T. Asano, Y. Tanaka, and S. Noda, Appl. Phys. Lett. **82**, 1341 (2003).
[25] J. Fu, S. He, and S. Xiao, J. Phys. A **33** 7761 (2000).
[26] T. Asano, B. Song, Y. Tanaka, and S. Noda, Appl. Phys. Lett. **83**, 407 (2003).
[27] S. Kim, I. Park, and H. Lim, Opt. Express **12**, 5518 (2004).
[28] A. Chutinan, M. Mochizuki, M. Imada, and S. Noda, Appl. Phys. Lett. **79**, 2690 (2001).
[29] Z. Wang and S. Fan, Phys. Rev. E **68**, 066616 (2003).
[30] K. S. Yee, IEEE Trans. Antennas Propag. **14**, 302 (1966).
[31] A. Taflove, in *Computational Electrodynamics: The Finit-Difference Time-Domain Method* (Artech House, Norwood, 2000), 2nd edition.
[32] R. Grover, T. A. Ibrahim, S. Kanakaraju, L. Lucas, L. C. Calhoun, and P. T. Ho, IEEE Photon. Technol. Lett. **16** 467 (2004).
[33] J. A. Wahl, J. S. V. Delden, and S. Tiwari, IEEE Photon. Technol. Lett. **16** 1873 (2004).
[34] H. Cao, C. Liu, H. Ling, H. Deng, M. Benavidez, V. A. Smagley, R. B. Caldwell, G. M. Peake, G. A. Smolyakov, P. G. Eliseev, and M. Osiński, Appl. Phys. Lett. **86**, 041101 (2005).
[35] W. Mao, P. A. Andrekson, and J. Toulouse, IEEE Photon. Technol. Lett. **17** 420 (2005).
[36] C. Yeh and L. A. Bergman, Phys. Rev. E **60**, 2306 (2004).
[37] C. Etrich, N. C. Panoiu, D. Mihalache, and F. Lederer, Phys. Rev. E **63**, 016609 (2000).
[38] P. Lodahl, A. F. van Driel, I. S. Nikolaev, A. Irman, K. Overgaag, D. Vanmaekelbergh, and W. L. Vos, Nature (London) **430**, 654 (2004).
[39] T. D. Happ, I. I. Tartakovskii, V. D. Kulakovskii, J. P. Reithmaier, M. Kamp, and A. Forchel, Phys. Rev. B **66**, 041303(R) (2002).
[40] Z. Y. Li, L. L. Lin, and Z. Q. Zhang, Phys. Rev. Lett. **84**, 4341 (2000).
[41] M. Florescu and S. John, Phys. Rev. A **69**, 053810 (2004).
[42] J. Vuckovi, M. Pelton, A. Scherer, and Y. Yamamoto, Phys. Rev. A **66**, 023808 (2002).
[43] K. M. Ho, C. T. Chan, and C. M. Soukoulis, Phys. Rev. Lett. **65** 3152 (1990).
[44] D. Cassagne, C. Jouanin, and D. Bertho, Phys. Rev. B **53**, 7134 (1996).
[45] Z. Y. Li, J. Wang, and B. Y. Gu, Phys. Rev. B **58**, 3721 (1998).
[46] J. B. Pendry, J. Mod. Opt. **41**, 209 (1994).
[47] L. Li, J. Opt. Soc. Am. A **13**, 1024 (1996).
[48] Z. Y. Li and L. L. Lin, Phys. Rev. E **67**, 046607 (2003).
[49] Z. Y. Li and K. M. Ho, Phys. Rev. B **68**, 155101 (2003).
[50] Z. Y. Li and K. M. Ho, Phys. Rev. B **68**, 245117 (2003).
[51] Z. Y. Li, H. Y. Sang, L. L. Lin, and K. M. Ho, Phys. Rev. B **72**, 035103 (2005).
[52] N. A. Nicorovici, R. C. McPhedran, and L. C. Botten, Phys. Rev. E **52**, 1135 (1995).
[53] L. M. Li and Z. Q. Zhang, Phys. Rev. B **58**, 9587 (1998).
[54] L. C. Botten, N. A. Nicorovici, R. C. McPhedran, C. M. Sterke, and A. A. Asatryan, Phys. Rev. E **64**, 046603 (2001).